Physica Medica 103 (2022) 190–198

Contents lists available at ScienceDirect

Physica Medica

journal homepage: www.elsevier.com/locate/ejmp

Review paper

CTContour: An open-source Python pipeline for automatic contouring and calculation of mean SSDE along the abdomino-pelvic region for CT images; validation on fifteen systems

Eric Pace [a,*], Carmel J. Caruana [a], Hilde Bosmans [b], Kelvin Cortis [c], Melvin D'Anastasi [c], Gianluca Valentino [d]

[a] Medical Physics, Faculty of Health Science, University of Malta, Msida MSD2080, Malta
[b] Department of Medical Radiation Physics, University Hospital Leuven, Herestraat 49, Leuven B-3000, Belgium
[c] Medical Imaging Department, Mater Dei Hospital, Triq id-Donaturi tad-Demm, Msida MSD2090, Malta
[d] Communications & Computer Engineering Department, Faculty of Information and Communication Technology, University of Malta, Msida MSD2080, Malta

ARTICLE INFO

Keywords:
Size-specific dose estimate (SSDE)
Patient contour
Patient dose calculation software
Computed tomography (CT) doses
Water equivalent diameter (WED)
Truncation

ABSTRACT

Purpose: Calculation of the Size Specific Dose Estimate (SSDE) requires accurate delineation of the skin boundary of patient CT slices. The AAPM recommendation for SSDE evaluation at every CT slice is too time intensive for manual contouring, prohibiting real-time or bulk processing; an automated approach is therefore desirable. Previous automated delineation studies either did not fully disclose the steps of the algorithm or did not always manage to fully isolate the patient. The purpose of this study was to develop a validated, freely available, fast, vendor-independent open-source tool to automatically and accurately contour and calculate the SSDE for the abdomino-pelvic region for entire studies in real-time, including flagging of patient-truncated images.
Methods: The Python tool, CTContour, consists of a sequence of morphological steps and scales over multiple cores for speed. Tool validation was achieved on 700 randomly selected slices from abdominal and abdomino-pelvic studies from public datasets. Contouring accuracy was assessed visually by four medical physicists using a 1–5 Likert scale (5 indicating perfect contouring). Mean SSDE values were validated via manual calculation.
Results: Contour accuracy validation produced a score of four of five for 98.5 % of the images. A 300 slice exam was contoured and truncation flagged in 6.3 s on a six-core laptop.
Conclusions: The algorithm was accurate even for complex clinical scenarios and when artefacts were present. Fast execution makes it possible to automate the calculation of SSDE in real time. The tool has been published on GitHub under the GNU-GPLv3 license.

Introduction

The $CTDI_{vol}$ is a standardised dose metric for quantifying radiation detriment from CT scanners and defined on cylindrical PMMA phantoms of either 16 or 32 cm diameter [1]. This metric was not intended as a valid descriptor of patient dose and certainly not in the case of different sized patients. AAPM working group 204 (AAPM204) [2] published guidance on how simple-to-measure patient body habitus descriptors, measured on the CT images themselves, may be used in conjunction with the $CTDI_{vol}$ to obtain an appropriate patient size specific dose estimate (SSDE). The first body habitus metrics that were introduced for this purpose were the patient's posterior-anterior (PA) and lateral (LAT) diameters, and a subsequent effective patient diameter, defined as:

$$\text{Effective diameter} = \sqrt{PA \times LAT} \tag{1}$$

A more recent AAPM working group (AAPM220) [3] described an improved metric for patient habitus that is weighted by patient voxel attenuation coefficients relative to water. This metric is the Water Equivalent Diameter (D_w) and is given by:

$$D_w = 2\sqrt{\left[\frac{1}{1000}\overline{CT(x,y)}_{ROI} + 1\right]\frac{A_{ROI}}{\pi}} \tag{2}$$

* Corresponding author.
E-mail address: eric.pace.08@um.edu.mt (E. Pace).

https://doi.org/10.1016/j.ejmp.2022.10.027
Received 29 June 2022; Received in revised form 1 October 2022; Accepted 31 October 2022
Available online 11 November 2022

where $\overline{CT(x,y)_{ROI}}$ is the mean pixel value and A_{ROI} is the cross-sectional area of the patient as measured in the CT slice. AAPM220 subsequently recommended that D_w be used in place of the effective diameter for calculating the SSDE when using the conversion factors specified in AAPM204.

AAPM220 further recommends that D_w and subsequently SSDE be calculated for every CT slice. A single representative SSDE value, in mGy, for the entire scan may then be determined by averaging over all the slices:

$$\overline{SSDE} = \frac{\sum_{z=1}^{N} SSDE(z)}{N} \quad (3)$$

where N is the total number of slices. If it is not feasible to process every single slice, AAPM220 recommends choosing subsets of slices at intervals along the z-axis that do not exceed 5 mm. It has also been suggested that a single representative 'central slice' may be acceptable in certain cases [4–6]. However, ideally all slices should be used and averaged. The AAPM recommendation that D_w be evaluated at every CT slice is, for routine real-time applications and bulk processing, too time intensive if only manual contouring is available; an automated approach is therefore desirable.

Existing approaches for patient contouring

Determination of the patient's outline requires exclusion of the surrounding air, the patient couch and mattress as well as any other non-patient objects. AAPM220 describes a single-step approach of setting a threshold of −383HU to exclude the patient couch. However, in some cases, parts of the couch would still be visible together with a thin portion of the top surface of the mattress trailing very close to the patient, requiring further morphological steps to remove completely. An example of this is shown in region A of Fig. 1. Alternate patient contour studies employing a threshold value of −200HU [6] minimised this issue. Other work on automated contouring first removed the couch, then applied a threshold of −900HU to exclude any artefacts with low CT numbers [4]. However, it is not clear what processes were performed to remove the couch, and applying a threshold of −900HU directly on the input image sometimes resulted in the patient trunk being connected to the couch. This is illustrated in region B of Fig. 1.

Automated contouring tools should also be able to identify slices having patient truncation artefacts, i.e. where the patient region falls beyond the reconstructed FOV (FOV) or beyond the edge of the image matrix, since AAPM220 does suggest that such slices be excluded from the computation of the mean SSDE. A problem with the earlier mentioned threshold of −200HU was that sometimes jagged contours were produced on truncated slices, which may impede the process of truncation detection. This is shown in region C of Fig. 1.

Other approaches of varying complexity are described in the literature. Gharbi et al (2020) proposed a clustering algorithm tested on anthropomorphic phantoms [7]. Anam et al (2016) used morphological operations also validated on anthropomorphic phantom images [6]. Boos et al (2017) addressed full patient cases and performed automated thresholding to obtain an initial set of segmented contours. These regions were subsequently filled in and the single largest contour in a given slice was considered to be the patient outline [8]. Burton and Szczykutowicz (2018) drew circular contours inscribed in the square pixel array and remapped any padding pixels to a value of −1000HU, without performing any further morphological steps [9]. Özsoykal et al (2018) performed thresholding between −1000HU and 3000HU to

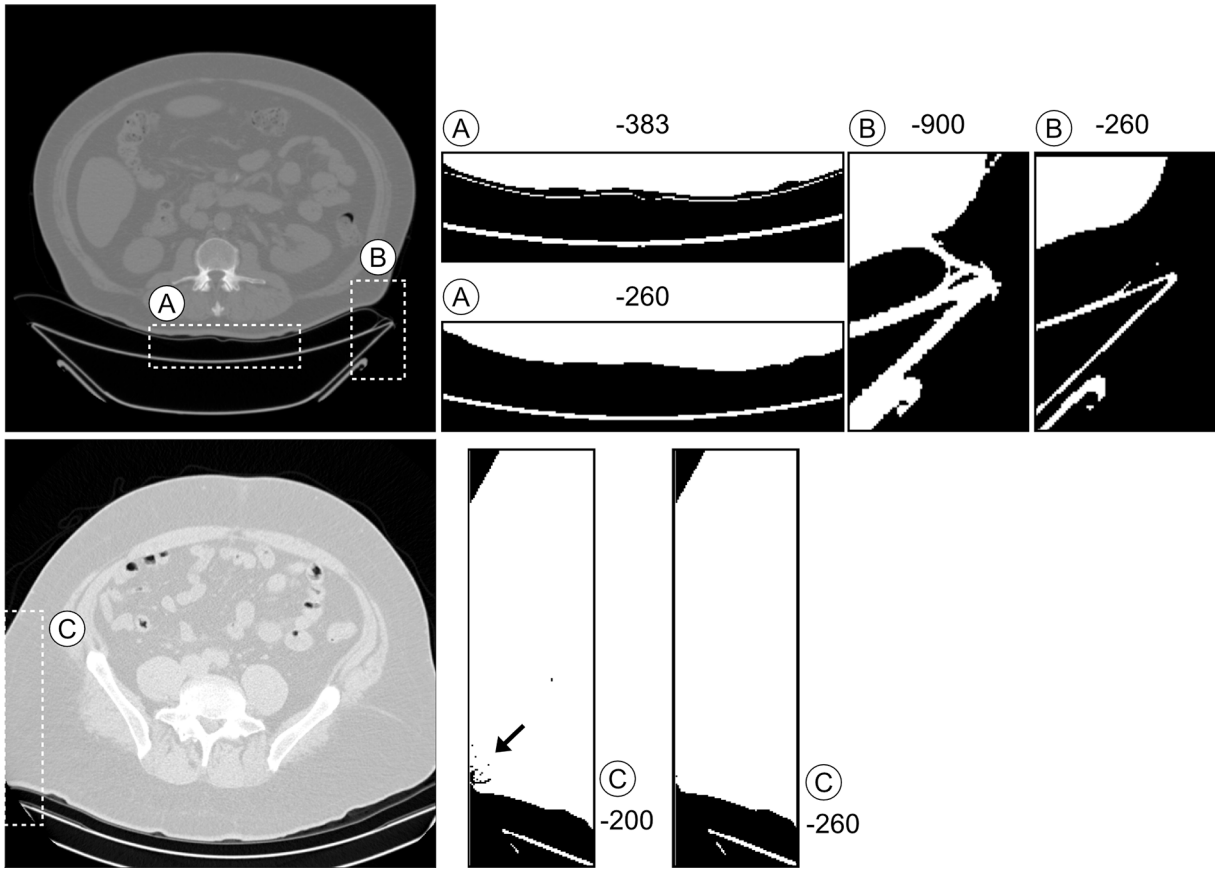

Fig. 1. Potential of undesirable effects at different threshold values which are alleviated with a threshold value of −260HU. Original images at left indicating areas of focus. Areas at right show thresholding result with threshold value on top of image. Possibility of (A) top part of mattress to be included, (B) patient trunk being connected to couch, and (C) jagged contours.

isolate patient anatomy [10]. More recent work by Anam et al (2021) proposed a detailed morphological process that performed thresholding, edge detection, selection of the largest six contours and removal of the patient table by considering the y-position of each contour [11,12]. A software tool developed as part of the MEDIRAD project, AutoWED [13], performed morphological opening with a 12-pixel square structuring element, followed by Otsu thresholding and filling. At the end, the algorithm retained the single largest determined contour as the patient contour. This tool is freely provided as an online service [14] however is limited to processing either a single slice or a specific set of slices at a time; since it requires users to upload their images to a remote server, this might be time intensive. The tool provides as a result the D_w value only, without making available the Boolean contour mask or the results of patient area and mean pixel value. Only Anam et al provided a detailed description of the processing pipeline used in their study. Therefore, an open-source, fully automated program based on a transparent pipeline that may be used to process entire datasets executed on a local machine is desirable to facilitate further research. To aid researchers the tool should be accompanied by clear details of the processing pipeline.

The purpose of this work was therefore to develop a validated, fast (exploiting multiple cores), freely available, open-source tool, to automatically and accurately contour the patient trunk across the abdomino-pelvic region and calculate the SSDE including cases when complex clinical anatomy and trunking artefacts are present.

Methods

The processing pipeline

A flowchart of the processing pipeline is shown in Fig. 2. Implementation was carried out in Python 3.8 using the Pandas 1.2.1, Pydicom 2.1.2, scikit-image 0.18.2, scipy 1.4.1, and numpy 1.18.1 libraries [15–20]. Each DICOM slice was first rescaled to obtain actual Hounsfield Units (HU) according to the equation:

$$\mathrm{HU} = \text{pixel value} \times \text{slope} + \text{intercept} \tag{4}$$

The slope and intercept values were obtained from the DICOM tags *Rescale Slope* and *Rescale Intercept*.

The pixel data were then passed to the contouring process. Since the thresholds found in the literature (−900HU [4], −383HU [3] and −200HU [6]) produced artefacts with some images, we experimented with various other threshold values and found that −260HU led to an elimination of the artefacts in these images (Fig. 1).

The morphological operations from thresholding to dilation were applied to the whole pixel array. *Despeckle* refers to the process of small object removal. The *despeckle-erode-despeckle* sequence removes very thin and small objects so that it is very effective in removing any remnant patient couch or any small non-patient objects.

Morphological erosion on a region in a binary image has the effect of pushing the perimeter of that region inwards, thereby reducing its area. This is a bitwise operation where a mask - known as a structuring element - is translated over each pixel in the original image. For a given pixel $p_{i,j}$ in the original image, the structuring element is centred over

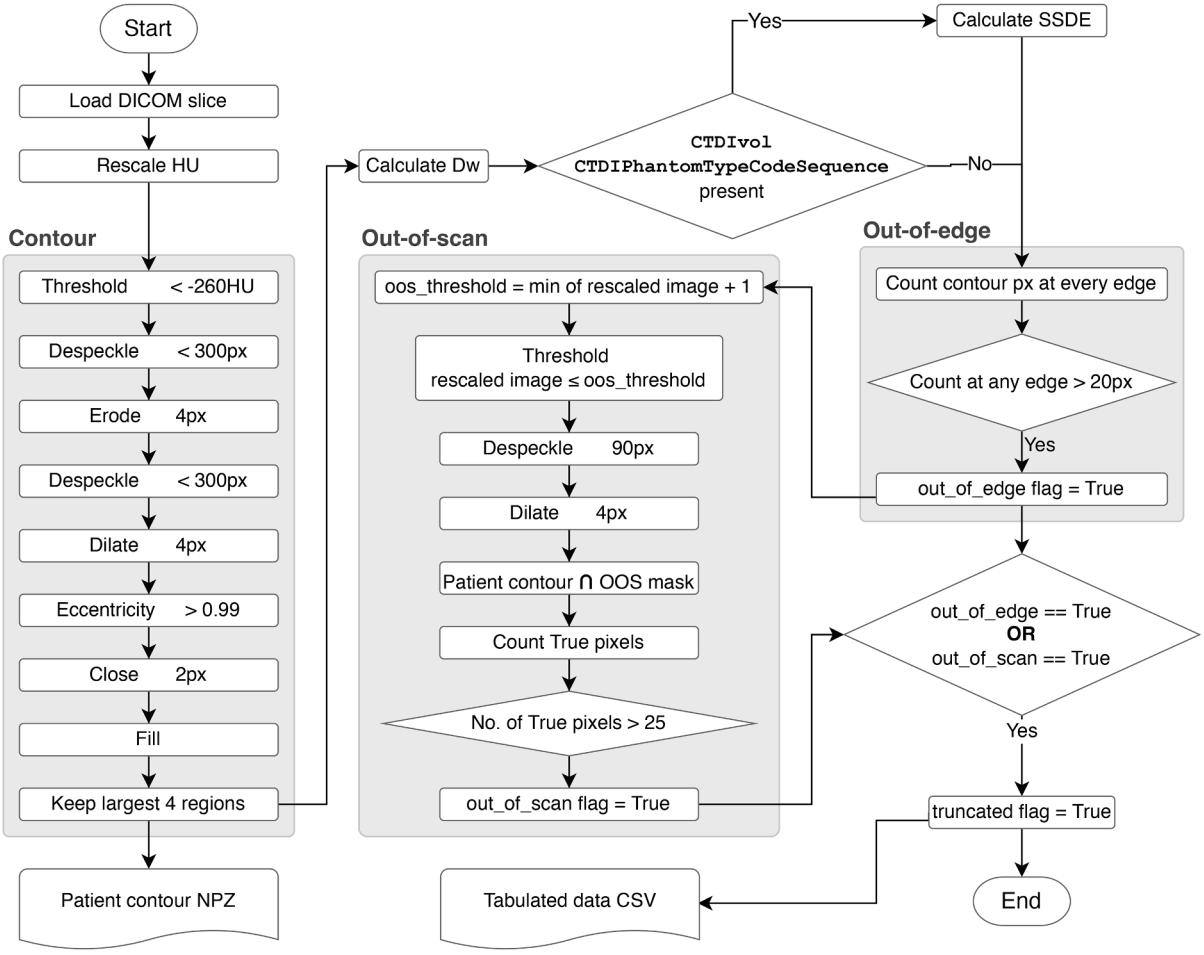

Fig. 2. Flowchart showing process to identify patient contours, out-of-edge truncation and out-of-scan truncation.

that pixel. If all the neighbouring pixels around $p_{i,j}$ in the binary image that are overlayed by the structuring element are 1, then pixel $p_{i,j}$ remains 1, else it is set to 0. The amount of erosion is determined by the shape and size of the applied structuring element, with increasing sizes resulting in greater erosion.

Dilation is defined as the reverse process of erosion. The dilation operation, using the same structuring element shape and size, is used to re-expand the regions' borders to recover any eroded patient boundary.

For the steps of erosion and dilation, a simple square structuring element was tested with a variety of sizes: 2, 4, 6, px sides. A square structuring element of sides 4px is shown in Fig. 3A. The 2 × 2px element did not manage to fully erode the patient couch in all images, with final images including remnant non-patient regions that result in an over-estimation of the patient area. This is illustrated in Fig. 4A. Increasing the size to 4 × 4px resolved this issue, but moving to higher sizes (6 × 6 and 8 × 8px, respectively) did not provide any further improvement. Hence for this work a square structuring element with size 4 × 4px was chosen.

Dilation sometimes resulted in thin arc remnants of the patient couch (Fig. 5, centre image). To eliminate these, an eccentricity filter was used. For each contour, an eccentricity value was calculated which assumed the contour shape to be elliptical, with the eccentricity being defined as:

$$e = \frac{c}{a} \tag{5}$$

where c is the distance from the centre of the ellipse to one of the foci, and a is the length of the semi-major axis. Contours with an eccentricity value ≥ 0.99 such as highly elongated remnants of the patient couch not removed in the previous steps were thus eliminated.

The effect of *closing* (filling-in) is to bridge small undesired gaps between regions (e.g. fat folds that lay close to the main trunk but happen to be separated by a thin air boundary would be connected together). Morphological closing is defined as a morphological dilation followed immediately by a morphological erosion, with both morphological steps using the same structuring element shape and size - this is important to ensure the region boundary is unchanged by the close operation operation. The shape and size of the structuring element determines the maximum gap size that could be closed, with higher element sizes increasing this closable gap.

For the step of morphological closing, the use of simple square structuring elements were noted to leave undesirable small non-smooth nooks in the contour at the boundary of the filled-in region where gaps would have been closed (see arrows in Fig. 4B).

For this reason, a circular structuring element was preferred. For this work, a radius of 2px was found to lead to the most representative contour around the patient. This is illustrated in Fig. 4B, while the structuring element is shown in Fig. 3B.

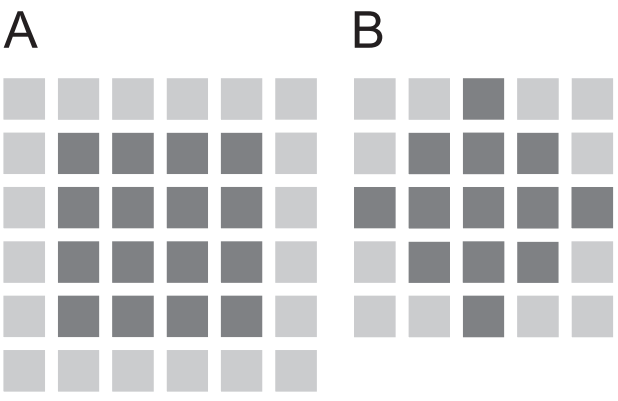

Fig. 3. Structuring elements generated by the morphology module of the scikit-image library as used in this work [18]. (A) is a square of side 4 pixels (B) is a disc of radius 2 pixels. Dark squares are True (or 1), light squares are False (or 0).

Finally the *fill* operation filled any hollow areas within each region (such as gas in intestine). From this final set of contours, the largest four were selected.

The result of the contouring function was a Boolean mask containing up to four contours covering the patient's abdomino-pelvic trunk and other patient anatomy present in the slice.

Calculation of D_w and SSDE

The identified final mask was used to determine the area and mean pixel value of the CT slices. This permitted the calculation of D_w. Furthermore, for systems that had relevant CTDIvol and phantom diameter stored as part of the DICOM header, a calculation of the SSDE was possible, using the above equations from the AAPM204 report. Processing all slices in the study produced a list of SSDE values which were then averaged to obtain a single representative average SSDE value. The tool produced tabulated results with a row for each slice with the following fields: slice name, D_w (mm2), mean pixel value (HU), CTDIvol (mGy) if the CTDIvol DICOM tag was available and SSDE if the phantom diameter DICOM tags was also available.

Detection of slices with truncated patient anatomy

Truncated patient anatomy may be due to either or both of the following: 'out-of-scan truncation', defined as patient anatomy extending beyond the reconstructed circular FOV and 'out-of-edge' truncation, which may be defined as the patient anatomy extending beyond the displayed square FOV. Examples of both types of truncation are shown in Fig. 6A and B respectively. This tool was developed to identify both truncation types. Thus separate flags were defined for out-of-scan and out-of-edge truncation. A final 'truncation' flag is set to true if either or both of the above flags are set to true. The approach depends on the patient contour having already been established.

Detection of out-of-edge truncation was performed by counting the number of pixels of the resulting patient contour on the leftmost and rightmost column of pixels, and on the topmost and bottommost row of pixels. A threshold was set per edge – in this manner, each edge is tested independently for truncation. A threshold value of 20 pixels was found to reliably omit any false negatives in the case the patient anatomy only tangentially touches the edge of the image.

Detection of out-of-scan truncation was performed by first determining the out of scan region. In this work, this was defined as any pixel with a value less than or equal to the minimum pixel value of the image plus 1. A mask of these pixels was generated and a *despeckle* operation was applied to remove objects smaller than 90 pixels. A *dilation* operation was then performed using a 4px-square structuring element such that the resulting mask extended into the FOV by a thin margin.

A Boolean intersection of the patient contour and this out-of-scan mask was then applied, producing an 'out-of-scan map' that highlighted any patient regions that were in contact with the out-of-scan mask. A threshold of 25 pixels was applied to this out of scan map to again avoid false negatives.

The tool adds these three truncation flags as part of the final output. Visual representation of the truncation boundaries for both types of truncation are shown in Fig. 6C and D.

Tool validation

For validation, the tool was tested on two separate datasets.

The first dataset included a wide variety of patient anatomical presentations and variety of table couch and mattress structures. This dataset was the Climb 4 Kidney Cancer Kidney Tumor Segmentation Challenge 2019 (C4KC-KiTS) available on The Cancer Imaging Archive, an online public domain database of studies [21–23]. Filtering this dataset for abdomen and pelvis images yielded 138 studies which had

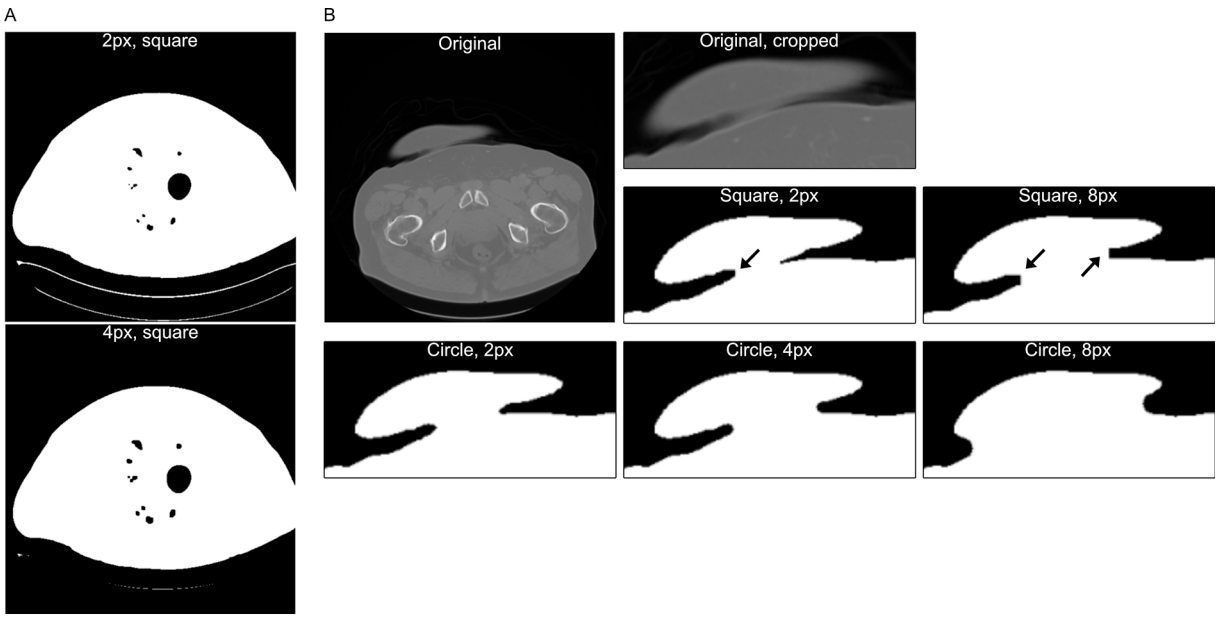

Fig. 4. Effect of structuring element shape and size. 4A shows the erosion and dilation steps using a square structuring element with sides of 2px (top) and 4px (bottom). The former does not fully erode the patient couch. 4B shows the closing step on a slice containing a fat fold over the patient's top-left abdomen. The middle row used a square structuring element with sides 2px and 8px. In both cases, the 'bridge' of the merged fat fold had a distinct non-smooth nook (indicated with arrows). The bottom row used a circular structuring element with radii 2, 4, 8px. In these cases, the bridged contour was noted to be smoother than when square elements were used. The 2px circular structuring element provided the best contour.

been conducted on fifteen systems as identified by the Manufacturer Model Name tag in the DICOM header from three manufacturers: Siemens, Toshiba and Philips.

The second dataset was the Stage-II Colorectal-CT [21,24,25] dataset, also available from The Cancer Imaging Archive. This dataset provided contrast enhanced abdomino-pelvic images of 230 patients prior to surgery where imaging was carried out on four Siemens and Philips systems.

A random sample of 700 of the contoured slices from the public datasets was independently assessed visually by four medical physicists (MP) each with more than 5 years' experience. MPs were asked to score the quality of the contour on a 5-point Likert scale. A value of five indicated perfect contouring, a value of four indicated quasi-perfect contouring of the trunk outline (error in patient cross-sectional area less than 5 %), a value of three indicated minor false contours (error in patient cross-sectional area less than 10 %), a value of two indicated major false contours (error in patient cross-sectional area higher than 10 %), a value of one indicated that the patient trunk was not contoured at all.

The same random sample of images were manually checked for truncation (either out-of-scan or out-of-edge to check the accuracy for truncation detection.

As an additional check on the calculation of D_w and SSDE by CTContour, we took a random sample of 50 individual images, checked the contour visually for accuracy, read off the area and mean HU of the contoured image given by CTContour and then computed the D_w, conversion factor and SSDE manually using a calculator. The results were identical to those given by CTContour.

Parallel processing

Since slices may be processed independently of each other, it was easy to exploit parallel processing to take advantage of multiple CPUs. This was achieved using the Python function `starmap` from the `multiprocessing.Pool` module, which unravels the processing of each slice to run in parallel on all available processors.

Results

Fig. 5 shows the individual steps of the contour process. The bottom left image shows the extracted patient trunk from the original image. Fig. 7 shows patient contour results in white outline for a variety of systems and patient couches.

Pooling reviewers' responses together, 98.5 % of the images were given a score of either 4 or 5. Most of the images with a score of 4 were the result of a remnant meniscus from truncated abdomens.

The accuracy of the truncation detection approach, for both types of truncation combined, was found to be 98.9 % with zero false negatives and eight false positives out of a total of 700 images.

Processing speed

Table 1 shows the time (using `time.perf_counter()`) taken to contour a folder with 300 512x512px slices on an 6-Core Intel(R) Core (TM) i7-8850H CPU at 2.60 GHz. The software tool was written to allow the user to configure which operations and output is performed. Thus table 1 lists the time needed for common operations to separate out the time needed for I/O bound operations. NPZ refers to Numpy compressed file archive containing the patient contour binary mask with a size of 2 KB per slice.

Discussion

The aim of this work was to prepare a fully automated patient contouring tool that could evaluate the mean SSDE for a given CT study in the abdomino-pelvic region using the individual SSDE from all the slices, as recommended by the AAPM. In this work we presented a validated linear, deterministic sequence of processes to contour CT axial abdominal and abdomino-pelvic scans automatically that is capable of contouring a 300-slice study in just over 6 s. Further benefits of the approach chosen in this work is that by applying pixel-wise morphological processes, each step may be visualised and its effect inspected. The performance of the contouring process has been found to be extremely robust for the investigated studies over the variety of systems

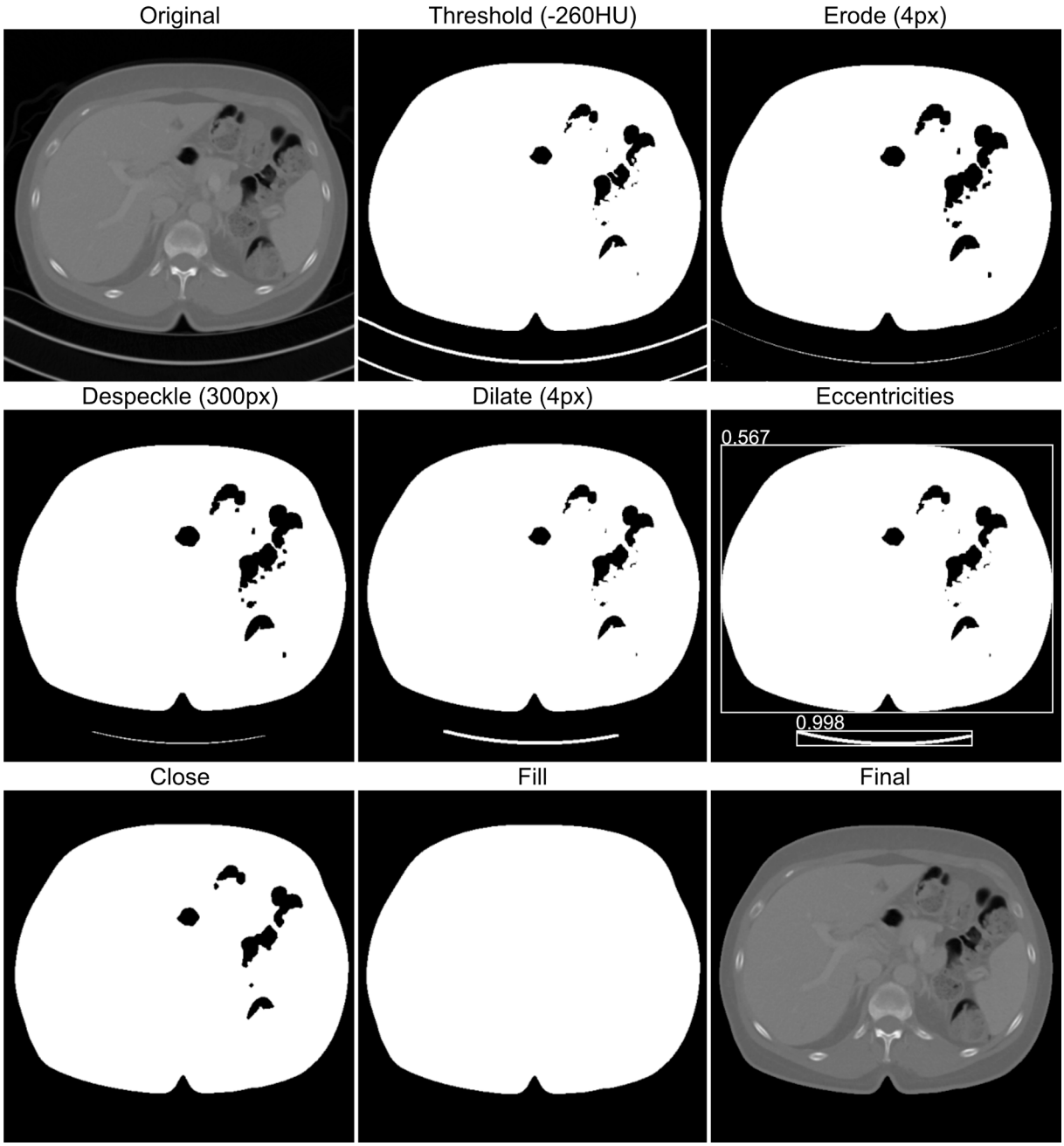

Fig. 5. Notable individual steps of the morphological process.

tested. The work was also implemented using free open-source tools and provided at no cost under a permissive license meaning that there is no cost-barrier in implementing this solution at any facility.

We compared our results with results obtained using AutoWED [14] and they were in very close agreement (over a sample of 700 slices, AutoWED gave a mean difference of + 0.2 %, statistically significant at $p < 0.001$ using a paired *t*-test). We did investigate outlier cases when the difference was higher than normal. These were invariably found to be the more difficult-to-contour cases. We checked our contours and they were very accurate so we assume our approach leads to better results in difficult cases. An example is shown in Fig. 8 (where AutoWED gave a result of 0.23 cm less than ours) in which there is a fat fold which is completely isolated from the main trunk. Since AutoWED retains only the largest contour as the patient, it may have ignored the fatfold. This may perhaps indicate that retaining more than one final contour is important, supporting our decision to keep the largest four contours.

Our approach for the detection of patient truncation had no false negatives indicating that the process did not miss any truncated images, whilst simultaneously maintaining a high accuracy. The number of false positives was low at the selected threshold values. Whilst higher threshold values might reduce slightly the false positives, there is potential for an increase in false negatives. Given the numerous borderline scenarios, the chosen threshold values were found to offer the best results.

Newer CT systems will increasingly be providing SSDE estimates as part of the patient dose report [26]. Dose monitoring platforms capable of evaluating the SSDE from topogram images are also available. It is nonetheless important to make an independent check of the SSDE provided by these systems using own software as part of the Medical Physics quality assurance programme [27], more so if commercial calculations are based on non-linear machine learning techniques [28,29]. Commercial tools are essentially black-boxes that will not usually provide

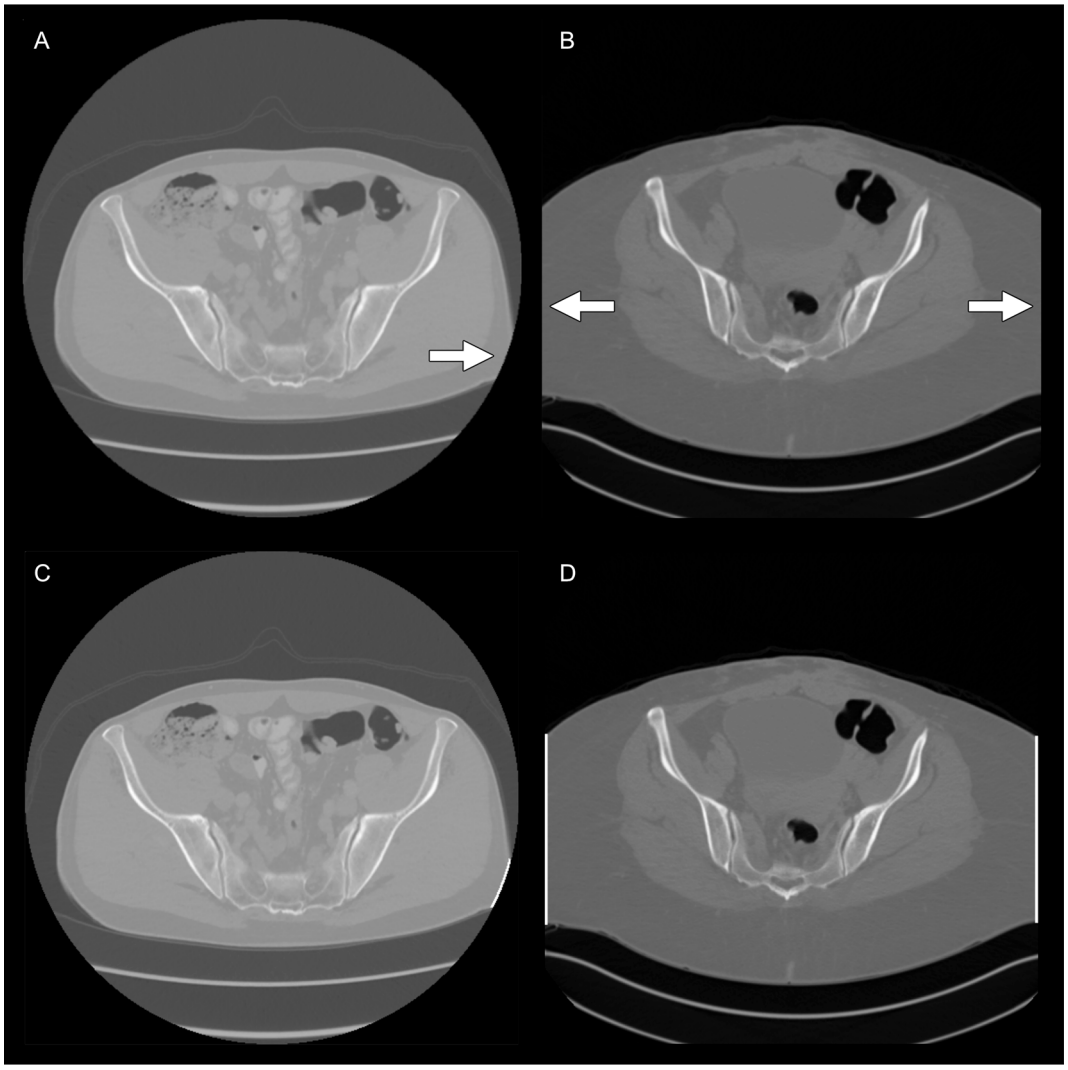

Fig. 6. Examples of the two types of truncation. (A) shows out-of-scan truncation, (B) shows out-of-edge truncation, (C, D) show detected truncation boundary in white over the original images A and B respectively using the tool described in this study.

Fig. 7. Examples of patient contour for a variety of patient couches. Patient outline is shown in white. For some systems, the reconstructed FOV diameter was larger than the displayed FOV resulting in part of patient table not being displayed entirely. In these cases the contour process still correctly excluded the patient table.

insight into the individual steps performed and may not necessarily provide a visual of each contoured slice to facilitate inspection. Finally, the availability of a boolean mask that isolates the patient region would serve as a useful precursor for further research that is not strictly limited to the determination of the SSDE.

Limitations and future work

There may be some scenarios where the performance of the contour process is not optimal. For example, it was noted that for a few of the images taken on the Siemens Sensation 64, a small part of the couch at

Table 1
Total time taken to contour 300 slices using one and six cores for a number of operations. Uncertainties are standard deviations from three repeated measurements. 'Truncation' refers to the truncation detection portion of the algorithm; csv and npz indicate file writing of these respective file types; merged csv indicates the merging of individual csv files into a single csv file, per folder.

Operation on 300 512 × 512px slices	Single core (s)	Multi-core (s)
Contour	13.9 ± 0.6	4.9 ± 0.1
Contour, truncation	16.3 ± 0.3	5.2 ± 0.1
Contour, truncation, csv	20.8 ± 0.4	6.3 ± 0.5
Contour, truncation, merged csv	21.8 ± 0.0	7.1 ± 0.2
Contour, truncation, merged csv, npz	24.1 ± 1.1	7.6 ± 0.8

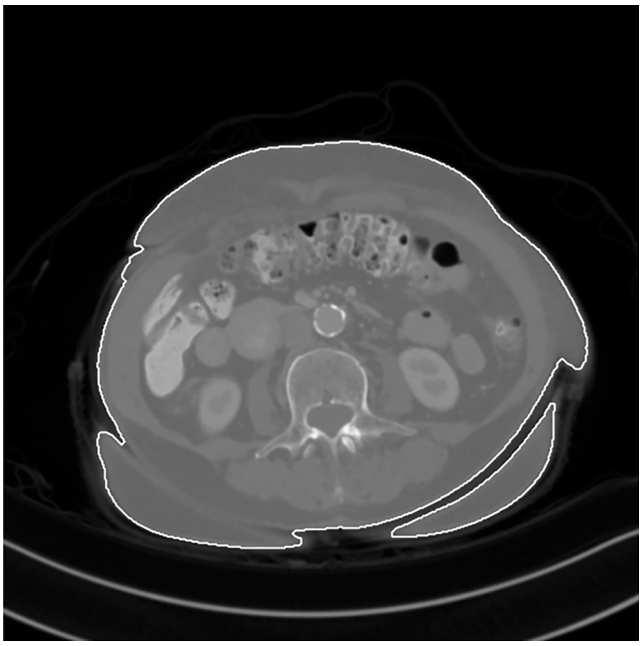

Fig. 8. Example of patient contour, shown as a white outline, using the method described in this work. A fat fold at the bottom-right of the patient trunk is contoured but unconnected to the patient trunk. Retaining more than the single largest contour ensures these patient portions are also included in the determination of D_w.

the rounded edges of either side was being included in the final contour. Repeating the contour process with a starting threshold of −383HU or −900HU did not provide better results. Contrarily, the number of contoured slices including this portion of the couch increased with these thresholds, with the −900HU threshold including nearly the entire couch. This couch portion was noted to typically have an area of 500-650px^2 with an eccentricity value of 0.85–0.92. The intention of this work was to provide a processing pipeline that remains system independent to facilitate multi-system and multi-centre studies. However, using this open-source algorithm the user would be able to adjust input parameters to each morphological process to fine-tune the performance of the contouring algorithm to their particular CT system if need be.

Conclusion

This work demonstrates that patient abdomino-pelvic trunk contouring on reconstructed axial slices may be automated with a very high accuracy for a wide variety of CT systems. This work also shows that the task may very easily be distributed on all system cores to allow for contouring to be carried out in close to real-time.

The validated tool was published on GitHub at https://github.com/ericpace/ctcontour under the GNU GPLv3 license together with installation and usage instructions.

Ethics

Only publicly available images data sets were used in this study.

Funding

This research did not receive any specific grant from funding agencies in the public, commercial, or not-for-profit sectors.

Declaration of Competing Interest

The authors declare that they have no known competing financial interests or personal relationships that could have appeared to influence the work reported in this paper.

References

[1] American Association of Physicists in Medicine. The Measurement, Reporting, and Management of Radiation Dose in CT. Report 96. 2008.
[2] American Association of Physicists in Medicine. Size-Specific Dose Estimates (SSDE) in Pediatric and Adult Body CT Examinations. Report 204. 2001.
[3] American Association of Physicists in Medicine. Use of Water Equivalent Diameter for Calculating Patient Size and Size-Specific Dose Estimates (SSDE) in CT. Report 220. vol. 2014. 2014.
[4] Leng S, Shiung M, Duan X, Yu L, Zhang Y, McCollough CH. Size-specific dose estimates for chest, abdominal, and pelvic CT: Effect of intrapatient variability in water-equivalent diameter. Radiology 2015;276:184–90. https://doi.org/10.1148/radiol.15142160.
[5] Daudelin A, Medich D, Andrabi SY, Martel C. Comparison of methods to estimate water-equivalent diameter for calculation of patient dose. J Appl Clin Med Phys 2018;19:718–23. https://doi.org/10.1002/acm2.12383.
[6] Anam C, Haryanto F, Widita R, Arif I, Dougherty G. Automated Calculation of Water-equivalent Diameter (DW) Based on AAPM Task Group 220. J Appl Clin Med Phys 2016;17:320–33. https://doi.org/10.1120/jacmp.v17i4.6171.
[7] Gharbi S, Labidi S, Mars M. Automatic brain dose estimation in computed tomography using patient dicom images. Radiat Prot Dosimetry 2020;188:536–42. https://doi.org/10.1093/rpd/ncaa006.
[8] Boos J, Kröpil P, Bethge OT, Aissa J, Schleich C, Sawicki LM, et al. Accuracy of size-specific dose estimate calculation from center slice in computed tomography. Radiat Prot Dosimetry 2018;178(1):8–19. https://doi.org/10.1093/rpd/ncx069.
[9] Burton CS, Szczykutowicz TP. Evaluation of AAPM Reports 204 and 220: Estimation of effective diameter, water-equivalent diameter, and ellipticity ratios for chest, abdomen, pelvis, and head CT scans. J Appl Clin Med Phys 2018;19:228–38. https://doi.org/10.1002/acm2.12223.
[10] Ozsoykal I, Yurt A, Akgungor K. Size-specific dose estimates in chest, abdomen, and pelvis CT examinations of pediatric patients. Diagnostic Interv Radiol 2018;24(4):243–8. https://doi.org/10.5152/dir.2018.17450.
[11] Anam C, Mahdani FR, Dewi WK, Sutanto H, Triadyaksa P, Haryanto F, et al. An improved method for automated calculation of the water-equivalent diameter for estimating size-specific dose in CT. J Appl Clin Med Phys 2021;22(9):313–23. https://doi.org/10.1002/acm2.13367.
[12] Anam C, Arif I, Haryanto F, Widita R, Lestari FP, Adi K, et al. A simplified method for the water-equivalent diameter calculation to estimate patient dose in CT examinations. Radiat Prot Dosimetry 2019;185(1):34–41. https://doi.org/10.1093/rpd/ncy214.
[13] Stratakis J, Myronakis M, Damilakis J. MEDIRAD. Implications of Medical Low Dose Radiation Exposure. Software tool (CT-IQURAD) module on radiation dose. 2021.
[14] MEDIRAD Project. Automatic Calculation of Water-Equivalent Diameter 2022. http://ctdose-iqurad.med.uoc.gr/autowed/ (accessed April 24, 2022).
[15] van Rossum G, Fred L D. Python 3 Reference Manual. CreateSpace; 2009.
[16] The pandas development team. pandas-dev/pandas: Pandas 1.2.1 (v1.2.1) 2021. doi:10.5281/zenodo.4452601.
[17] Mason D, Scaramallion, Rhaxton, Mrbean-bremen, Suever J, Vanessasaurus. pydicom/pydicom: pydicom 2.1.2 (v2.1.2) 2020. doi:10.5281/zenodo.4313150.
[18] Van Der Walt S, Schönberger JL, Nunez-Iglesias J, Boulogne F, Warner JD, Yager N, et al. Scikit-image: Image processing in python. PeerJ 2014;2014:1–18. https://doi.org/10.7717/peerj.453.
[19] Virtanen P, Gommers R, Oliphant TE, Haberland M, Reddy T, Cournapeau D, et al. SciPy 1.0: fundamental algorithms for scientific computing in Python. Nat Methods 2020;17(3):261–72. https://doi.org/10.1038/s41592-019-0686-2.
[20] Harris CR, Millman KJ, van der Walt SJ, Gommers R, Virtanen P, Cournapeau D, et al. Array programming with NumPy. Nature 2020;585(7825):357–62. https://doi.org/10.1038/s41586-020-2649-2.
[21] Clark K, Vendt B, Smith K, Freymann J, Kirby J, Koppel P, et al. The Cancer Imaging Archive (TCIA): maintaining and operating a public information repository. J Digit Imaging 2013;26(6):1045–57. https://doi.org/10.1007/s10278-013-9622-7.
[22] Heller N, Isensee F, Maier-Hein KH, Hou X, Xie C, Li F, et al. The state of the art in kidney and kidney tumor segmentation in contrast-enhanced CT imaging: Results

of the KiTS19 challenge. Med Image Anal 2021;67:101821. https://doi.org/10.1016/j.media.2020.101821.
[23] Heller N, Sathianathen N, Kalapara A, Walczak E, Moore K, Kaluzniak H, et al. Data from C4KC-KiTS. Cancer Imaging Arch 2019. https://doi.org/10.7937/TCIA.2019.IX49E8NX.
[24] Tong T, Li M. Abdominal or pelvic enhanced CT images within 10 days before surgery of 230 patients with stage II colorectal cancer (Stage II-Colorectal-CT) [Dataset]. *Cancer Imaging Arch* 2022. doi:10.7937/p5k5-tg43.
[25] Li M, Gong J, Bao Y, Huang D, Peng J, Tong T. Prognosis prediction for stage II colorectal cancer by fusing computed tomography radiomics and deep-learning features of primary lesions and peripheral lymph nodes. Int J Cancer 2022. https://doi.org/10.1002/ijc.34053.
[26] International Electrotechnical Commission. IEC62985:2019. Methods for calculating size specific dose estimates (SSDE) for computed tomography. 2019.
[27] Theano E, Fitousi N, Bosmans H. Quality assurance of dose management systems. Phys Med 2022;99:10–5. https://doi.org/10.1016/j.ejmp.2022.05.002.
[28] Bosmans H, Zanca F, Gelaude F. Procurement, commissioning and QA of AI based solutions: An MPE's perspective on introducing AI in clinical practice. Phys Med 2021;83:257–63. https://doi.org/10.1016/j.ejmp.2021.04.006.
[29] Kortesniemi M, Tsapaki V, Trianni A, Russo P, Maas Ad, Källman H-E, et al. The European Federation of Organisations for Medical Physics (EFOMP) White Paper: Big data and deep learning in medical imaging and in relation to medical physics profession. Phys Med 2018;56:90–3. https://doi.org/10.1016/j.ejmp.2018.11.005.